Ruthenium-driven catalysis for sustainable water decontamination: a review

Shengqi Zhang, Kaiting Zhang, Yuwei Xie, Yao-Yin Lou, Eric Lichtfouse, Mingbao Feng, Virender K Sharma

Ruthenium-driven catalysis for sustainable water decontamination: a review

Shengqi Zhang[1] · Kaiting Zhang[1] · Yuwei Xie[1] · Yao-Yin Lou[2] · Eric Lichtfouse[3] · Mingbao Feng[1] · Virender K. Sharma[4]

Abstract

The worldwide demand for clean water is rising worldwide, yet wastewater decontamination is actually limited by the pres-ence of refractory organic and inorganic compounds, calling for more efficient treatment methods. Here we review the use of ruthenium-based catalysts for the removal or transformation of pollutants at a concentration range of 1.0–100 mg/L under acid or neutral conditions. We focus on catalytic oxidation and reduction, and on the environmental impact of ruthenium catalysts. We discuss electrooxidation, photocatalytic oxidation, activation of inert oxidants, hydrogen-assisted reduction, electroreduction, and N–O bond activation.

Keywords Ruthenium · Catalytic redox reaction · Organic contaminants · Reaction mechanisms · Environmental catalysis

Introduction

Water contamination has increasingly become a critical issue threatening ecological safety and public health because of the continuous input of various synthetic organic compounds into global water (Kümmerer et al. 2018; Izzudin et al. 2021; Yang et al. 2022; Peng et al. 2023). The structural stability of organic pollutants with trace-level prevalence leads to degradation recalcitrance during conventional biological and chemical water treatments (Mutalib and Jaafar 2022). The discharge of the wastewater with those organic pollutants would degrade water quality. Thus, those wastewaters cannot be directly used for potable water (via desalination) and industrial applications only if more advanced technologies were performed to complete elimination of those organic pollutants. Therefore, green and highly efficient treatment strategies for wastewater decontamination have attracted worldwide attention, including thermal, membrane-based, chemical, and electrochemical technologies (von Gunten 2018; Hodges et al. 2018; Ying and Pumera 2019). As a multivalence transition metal ranging from 0 to VIII, ruthenium (Ru) has exhibited outstanding catalytic performances in (bio)chemical reactions such as photocatalytic ammonia synthesis (Yin et al. 2022), photoredox catalysis (Angerani and Winssinger 2019), water splitting (Axet and Philippot 2020), anodic hydrogen oxidation (Zhang et al. 2022), selective semi-hydrogenation of alkyne (Peil et al. 2022; Sanz-Navarro et al. 2022), and chemo-phototherapy (Xu et al. 2022), although all Ru compounds are regarded as toxic and as carcinogenic (Axet and Philippot 2020).

Regarding water treatment, studies have suggested that Ru-based materials could be employed as excellent catalysts for the reductive/oxidative elimination of environmental contaminants in the low-strength wastewater, listed in

Shengqi Zhang and Kaiting Zhang have authors contributed equally.

Yao-Yin Lou
yylou@xmu.edu.cn

Virender K. Sharma
vsharma@tamu.edu Eric Lichtfouse
eric.lichtfouse@icloud.com

[1] College of the Environment & Ecology, Xiamen University, Xiamen 361100, People's Republic of China

[2] State Key Laboratory of Physical Chemistry of Solid Surfaces, College of Chemistry and Chemical Engineering, Xiamen University, Xiamen 361005, People's Republic of China

[3] State Key Laboratory of Multiphase Flow in Power Engineering, Xi'an Jiaotong University, Xi'an 710049, Shaanxi, People's Republic of China

[4] Department of Environment and Occupational Health, School of Public Health, Texas A&M University, College Station, TX 77843, USA

Table 1 (Silva et al. 2007). Recent reviews have focused on the applications of Ru-based composites in aerobic amine oxidation (Ray et al. 2018), photoredox catalysis in chemical biology (Angerani and Winssinger 2019), cyclization of heteroatom-functionalized alkynes (Chung et al. 2020), hydrogen evolution reactions (Bae et al. 2020), and supercapacitors (Majumdar et al. 2019). Unfortunately, a detailed review of their applications in environmental catalysis for water decontamination has not yet been written. Therefore, the objectives of this minireview are to (1) summarize recent advances in Ru-based materials for environmental catalysis in the field of water purification, (2) provide a comprehensive and integrated analysis of the reactive oxidizing species and catalytic mechanisms during reduction or oxidation processes in Ru-driven treatment systems for pollutant removal, and (3) propose future perspectives on the development and application of Ru-based environmental catalysis for sustainable water treatment. Overall, this review has engineering implications for the chemical design and reactivity modulation of Ru-driven catalysts for efficiently remediating polluted environmental water.

Physical and chemical properties of ruthenium

Ruthenium as one of the platinum group metals does not tarnish at room temperatures but oxidizes in the air at about 800 °C. Ruthenium dissolves in fused alkalis to give ruthenates (RuO_4^{2-}). It is not attacked by acids (even aqua regia) but by halogens at high temperatures. The solubility limit of RuO_2 was 460 ppm by weight. In the range $0 < pH < 14$, Ru(II), Ru(V), Ru(VI), and Ru(VII) exist as Ru(II), Ru_2O_5 (s), RuO_4^{2-}, RuO_4^{-}, respectively (Fig. 1).

Catalytic oxidation

Electrooxidation

Ruthenium-based composites have been widely investigated as electrocatalysts for the electrochemical abatement of environmental pollutants in aquatic environments (León et al. 2021; Sun et al. 2022). Nitroaromatic compounds are used in industries and agriculture as explosives, pesticides, pharmaceuticals, polymers, synthesis of dyes, and other high-volume chemicals, which exhibit high toxicity and/or mutagenic activities in several living organisms and also widely present in many industrial wastewaters. Ruthenium was widely reported as a good electrocatalysts for electrooxidation of those toxic organic pollutants in the wastewater. For example, Kumar et al. (2015) and Chauhan et al. (2016) applied a highly stable Ti/RuO_2 electrode for the electrooxidation of nitrophenol and 4-chlorophenol (Kumar et al. 2015; Chauhan et al. 2016). The maximum removal of chemical oxygen demand and total organic carbon of nitrophenol solutions reached 99% and 82%, respectively (Table 1). Comparatively, the optimized chemical oxygen demand and 4-chlorophenol removal efficiencies were 96% and 97%, respectively (Table 1). Kinetic analysis suggested that the decomposition of nitrophenol and 4-chlorophenol follows a pseudo-first-order kinetic model. The electrochemical oxidation of nitrophenol yielded various products, including quinine, benzoquinone, and low-molecular-weight organic acids (e.g., maleic acid, succinic acid, and oxalic acid). The reaction mechanisms for nitrophenol and 4-chlorophenol were proposed, based on contributions of anode surface-bound $^{\bullet}OH$-mediated direct oxidation and chloride radical-triggered indirect oxidation. Additionally, electrochemical treatment using the modified Ti/RuO_2-IrO_2-stannum oxide anode also resulted in ~ 96% chemical oxygen demand removal from pharmaceutical wastewater, with the energy consumption was 58.09 kW h/kgCOD under current density of 8 mA cm^{-2}, initial pH of 2, and air flow of 18 L min^{-1} (Zhang et al. 2021).

Nitrate (NO_3^-) pollution in groundwater is primarily caused by agricultural runoff, and its presence in drinking water has been linked to adverse health outcomes, including thyroid cancer and methemoglobinemia in infants (Su et al. 2021). Besides, over NO_3^- residue in the wastewater contributes to the eutrophication and the imbalance of global nitrogen cycle. Chauhan and Srivastava (2020) recently reported the electrochemical elimination of NO_3^- ions in wastewater using Ti/ruthenium oxide as the anode and iron as the cathode. The NO_3^- ions were electro-reduced to NO_2^- and NH_4^+ ions on the iron cathode and then oxidized in situ into N_2 by $^{\bullet}OH$, which was generated on Ti/RuO_2 as the anode. In the case of wastewater containing Cl^- ions, the NO_2^- and NH_4^+ intermediates were also oxidized by $ClO^{\bullet}$ (reactions 1–7) (Su et al. 2021). The $ClO^{\bullet}$ was formed from Cl^- oxidation by $^{\bullet}OH$ through a series of reactions (see reactions 8–15). In this electroreduction-oxidation coupled system, a high total nitrogen removal efficiency (51%) was obtained at pH 12.0 with the current density of 285.7 A m^{-2}, which also brought in the advantage of a negligible amount of sludge produced in comparison with conventional biological denitrification processes.

$$NH_4^+ + OCl^- \rightarrow NH_2Cl + H_2O \quad (1)$$

$$NH_4^+ + ClO^{\cdot} \rightarrow H_2N^{\cdot} + HClO + H^+ \quad (2)$$

$$H_2N^{\cdot} + HClO \rightarrow NHCl_2 + H^+ \quad (3)$$

Table 1 Ruthenium-driven environmental catalysis for water decontamination

Treatment	Compound	Reaction conditions	Rate constant	Removal efficiency	Reactive species	References
Catalytic reduction	Aqueous oxyanion	[Ru/C] = 0.5 g/L, $[ClO_3^-]_0$ = 1.0 mM, pH = 7.2, 1 atm H_2, reaction time = 30 min	0.17 min^{-1}	100%	Hydrogen chemisorption, Oxyanion reduction	Chen et al. (2017)
	Bromate	[RuO_2/BC] = 0.4 g/L, $[BrO_3^-]_0$ = 5 mg/L, pH = 2.0, T = 25 ± 2 °C, reaction time = 60 min	0.0786 min^{-1}	100%	Adsorption and reduction, RuO_2, RuO_3	Fan et al. (2019)
	Dye	[Ru-CPM] = 0.42 g/L, $[CV]_0$ = 0.071 mM, $[NaBH_4]_0$ = 11.67 mM, reaction time = 15 s	0.1791s^{-1}	100%	Adsorption, Interfacial electron transfer	Veerakumar et al. (2015)
	Gongo red dye	[SWNT-Ru] = 0.25 g/L, $[Gongo]_0$ = 0.02 mM, $[NaBH_4]_0$ = 5.0 mM, reaction time = 1.74 min	0.1 min^{-1}	76.6%	Electron transfer	Hemraj-Benny et al. (2018)
	N-Nitrosamine	[In-house Ru/Al_2O_3] = 0.1 g/L, $[NDMA]_0$ = 100.0 µM, pH = 6.0, T = 22 ± 0.5 °C, 1 atm H_2, reaction time = 30 min	1.8 min^{-1}	100%	Hydrogenation	Huo et al. (2018)
	Nitrate	[Ru/C] = 0.2 g/L, $[NO_3^-]_0$ = 1.6 mM, 1 atm H_2, pH = 5.0, reaction time = 80 min	0.8 min^{-1}	100%	Hydrogenation	Huo et al. (2017)
	Nitrite	[Ru/C] = 0.2 g/L, $[NO_2^-]_0$ = 1.6 mM, pH = 5.0, 1 atm H_2, reaction time = 120 min	0.29 min^{-1}			
Catalytic oxidation	Atrazine	[Ru/TiO_2] = 1.0 g/L, $[ATZ]_0$ = 0.3 mg/L, $[Ozone]_0$ = 2.0 g/L, pH = 2.9 ± 1, T = 25 °C, reaction time = 17.5 min	–	100%	–	Biard et al. (2016)
	Azo-Dyes	[Si@p-RuNP] = 20 µL, $[CR]_0$ = 1.0 mM, $[H_2O_2]_0$ = 0.5 M, pH = 5.0, reaction time = 24 h	–	96%	·OH	Sahoo and Patra (2018)
	Butylparaben	[Ru/CeO_2] = 1.0 g/L, $[BP]_0$ = 25.0 µM, $[Mn(VII)]_0$ = 50.0 µM, pH = 7.0, T = 20 °C, reaction time = 40 min	0.135 min^{-1}	100%	Ru^{III}, Ru^{VI}, Ru^{VII}, ·OH	Zhang et al. (2013)
	Diclofenac	[CNRu] = 0.2 g/L, $[DCF]_0$ = 10.0 mg/L, $[Oxone]_0$ = 0.31 mM, pH = 3.80, reaction time = 10 min	0.334 min^{-1}	100%	$^1O_2$	Yan et al. (2022)
	E. coli	[Ru/NiFe-LDH] = 40 mg/L, [*E. coli*]$_0$ = 7 log cfu/mL, $[Oxone]_0$ = 5.0 mg/L, pH = 7.5, T = 25 °C, reaction time = 90 s	8.3 min^{-1}	100%	$^1O_2$	Zhou et al. (2022)
	Emerging pollutants	[Ru NPs] = 1.0 g/L, $[CMZ]_0$ = 25.0 µM, $[Mn(VII)]_0$ = 25.0 µM, pH = 7.0, T = 20 °C, reaction time = 10 min	0.03 min^{-1}	100%	Ru^{III}, Ru^{VI}, Ru^{VII}, ·OH	Zhang et al. (2014)
	Naproxen	[CNS-Ru] = 0.75 g/L, $[NPR]_0$ = 20.0 mg/L, $[H_2O_2]_0$ = 1.0 mM, pH = 7.0, T = 130 °C, P = 20 bar, reaction time = 120 min	0.69 min^{-1}	100%	·OH	Serra-Pérez et al. (2021)
	o-phenylenediamine	[Ru NPs] = 75 µg/mL, $[OPD]_0$ = 0.2 mM, $[H_2O_2]_0$ = 1.0 mM, reaction time = 20 min	0.35 min^{-1}	92%	An electron transfer intermediate	Cao et al. (2017)
	Organic contaminants	$[Ru^{III}]_0$ = 0.15 mM, $[DCF]_0$ = $[TCP]_0$ = 25.0 µM, $[Oxone]_0$ = 0.15 mM, pH = 3.0, T = 22 ± 2 °C	–	100%	Ru^V = O	Zong et al. (2021)

Table 1 (continued)

Treatment	Compound	Reaction conditions	Rate constant	Removal efficiency	Reactive species	References
	Organic contaminants	[RuO_2 NSs] = 0.125 g/L, [4-CP]$_0$ = 100.0 μM, [Oxone]$_0$ = 1.0 mM, pH = 7.0, reaction time = 10 min	–	100%	$SO_4^{\cdot-}$	Lim et al. (2019)
	Phenol	[RuO_2/Fe_3O_4@nSiO_2@mSiO_2] = 0.2 g/L, [PH]$_0$ = 50.0 mg/L, [Oxone]$_0$ = 1.0 g/L, pH = 7.0, T = 25 °C, reaction time = 40 min	–	100%	$SO_4^{\cdot-}$	Anbia and Rezaie (2017)
	Phenol	[RuO_2/AC] = 0.4 g/L, [PH]$_0$ = 50.0 mg/L, [Oxone]$_0$ = 1.0 g/L, pH = 7.0, T = 25 °C, reaction time = 20 min	0.174 min^{-1}	100%	$SO_4^{\cdot-}$	Muhammad et al. (2012)
	Phenol	[R-A-1 RuO_2/Al_2O_3] = 0.4 g/L, [PH]$_0$ = 50.0 mg/L, [Oxone]$_0$ = 2.0 g/L, pH = 7.0, *T* = 25 °C, reaction time = 60 min	–	100%	$SO_4^{\cdot-}$, $SO_5^{\cdot-}$	Anbia and Rezaie (2016)
	Sulfanilamide	[RuO_2-Rec] = 0.133 g/L, [SA]$_0$ = 58.0 μM, [H_2O_2]$_0$ = 1.16 mM, pH = 3.5, *T* = 25 °C, reaction time = 5 h	0.0084 min^{-1}	100%	$^{\cdot}OH$	Pan et al. (2021)
	Sulfamethoxazole	[RM] = 0.2 g/L, [SMX]$_0$ = 0.05 mM, [PAA]$_0$ = 1.0 mM, pH = 7.0, reaction time = 9 min	–w	100%	$CH_3C(O)O^{\cdot}$, $CH_3C(O)OO^{\cdot}$	Qian et al. (2022)
	Sulfamethoxazole	[Ru^{3+}]$_0$ = 100.0 μM, [SMX]$_0$ = 100.0 μM, [PAA]$_0$ = 0.2 mM, pH = 7.0 ± 0.1, *T* = 25 ± 1 °C, reaction time = 2.0 min	–	100%	$CH_3C(O)O^{\cdot}$, $CH_3C(O)OO^{\cdot}$	Li et al. (2021)
	Sulfamethoxazole	[Ru/ZSM-5A] = 0.5 g/L, [SMX]$_0$ = 5.0 μM, [Mn(VII)]$_0$ = 25.0 μM, pH = 7.0, *T* = 20 °C, reaction time = 30 min	14.77 M^{-1} s^{-1} g_{cat}^{-1}	100%	Electron shuttle	Zhang et al. (2015)
Electrocatalysis	Amoxicillin	Electrode = RuO_2/Ta_2O_5|Ti 30:70, [AMX]$_0$ = 0.1 mM, *j* = 15 mA, pH = 5.5, reaction time = 400 min	–	78%	$^{\cdot}OH$	León et al. (2021)
	Chlorophenol	DSA electrode = Ti/RuO_2, [4-CP]$_0$ = 100 mg/L, j = 222.22 A/m^2, pH = 5.2, reaction time = 180 min	0.0217 min^{-1}	97.2% COD = 96.7%	$^{\cdot}OH$, $Cl^{\cdot}$	Chauhan et al. (2016)
	N-nitrosodimethylamine	Electrode = Ru/CNT, [NDMA]$_0$ = 10.0 μM, potential = -0.9 V, pH = 6.0, reaction time = 120 min	563.9 μmol L^{-1} g_{Cat}^{-1} h^{-1}	100%	Direct electron transfer, H*	Sun et al. (2022)
	Pharmaceutical	Anode = RuO_2-IrO_2-SnO_2, [EA]$_0$ = 4179.921 mg/L, [EtOH]$_0$ = 18.02 g/L, *j* = 8 mA/cm^2, pH = 2.0, reaction time = 24 h	–	COD = 95.92%	H_2O_2	Zhang et al. (2021)
	p-nitrophenol	[Ti/RuO_2] = 300 mg/L, [PNP]$_0$ = 100 mg/L, *j* = 168.9 A/m^2, pH = 5.5, reaction time = 150 min	0.0285 min^{-1}	COD = 98.87%	$HO^{\cdot}$ adsorption	Kumar et al. (2015)
Photocatalytic oxidation	Antidepressant	[Ru-TNW] = 0.13 g/L, [TRA]$_0$ = 5.0 mg/L, pH = 5.8–6.2, reaction time = 8 h, Vis	–	88%	–	Osawa et al. (2020)

Table 1 (continued)

Treatment	Compound	Reaction conditions	Rate constant	Removal efficiency	Reactive species	References
	Chlortetracycline	[Ru3B] = 20 mg/L, $[CTC]_0$ = 25.0 mg/L, pH = 7.0, T = 298 K, reaction time = 240 min, SSL	29 min^{-1}	75%	$^1[O_2]$*	Salazar-Rábago et al. (2016a)
	Chlortetracycline	[X500Ru3B] = 1.0 g/L, $[CTC]_0$ = 25.0 mg/L, pH = 7.0, T = 25 °C, reaction time = 120 min, SSL	0.031 min^{-1}	70%	$^{\cdot}OH$, e_{aq}^-	Salazar-Rábago et al. (2016b)
	Cyclophosphamide	[Ru-TNW] = 0.13 g/L, $[CP]_0$ = 5.0 mg/L, pH = 7.5, reaction time = 34 min, UV–Vis	–	100%	–	Osawa et al. (2019)
	Ifosfamide	[Ru-TNW] = 0.13 g/L, $[IF]_0$ = 5.0 mg/L, pH = 7.5, reaction time = 27.6 min, UV–Vis	–	100%		
	Caffeine	[Ru-TNW] = 0.13 g/L, $[CF]_0$ = 20 mg/L, reaction time = 60 min, Vis	–	100%	$^{\cdot}OH$, $HO_2^{\cdot}$	Barrocas et al. (2019)
	Dye	$[Ru(bpy)_3^{3+}]_0$ = 1 µM, $[MO]_0$ = 12 mg/L, $[PS]_0$ = 2.0 mM, reaction time = 15 min	–	98%	$SO_4^{\cdot -}$, $^{\cdot}OH$	Subramanian et al. (2013)
	Dye	[Ru-doped TiO_2], $[dye]_0$ = 0.011 mM, pH = 1.0, E_{bias} = − 0.2 V, reaction time = 120 min, UV–Vis	–	98%	$^{\cdot}OH$, absorption	García-Ramírez et al. (2021)
	Emergent pollutants	[RuTNT] = 0.13 g/L, $[CA]_0$ = 20 mg/L, reaction time = 60 min, UV–Vis	–	100%	$^{\cdot}OH$	Barrocas et al. (2020)
	Methyl Blue	[RuC@g-C_3N_4/TiO_2] = 0.2 g/L, $[MB]_0$ = 10 mg/L, reaction time = 140 min, Vis	0.0336 min^{-1}	90%	$^1O_2$,$^{\cdot}OH$, $HO_2^{\cdot}$, H_2O_2	Jiang et al. (2018)
	Methyl Blue	[RuO_2-GO] = 0.1 g/L, $[MB]_0$ = 20 mg/L, reaction time = 60 min, UV–Vis	–	95%	$^{\cdot}OH$, $HO_2^{\cdot}$, hv	Akshatha et al. (2020)
	Phenazopyridine	[Ru(dcbpyH_2)$_2$$Cl_2$$TiO_2$] = 1.17 g/L, $[PAP]_0$ = 144 µM, reaction time = 60 min, UV–Vis	0.012 min^{-1}	55%	hole	Boyer et al. (2016)
	p-Nitrophenol	[RuPd/$H_x$$MoO_{3-y}$(200)] = 2.5 g/L, $[PNP]_0$ = 1.5 mM, T = 25 °C, reaction time = 5 min, H_2, UV–Vis	0.901 min^{-1}	100%	Active centers, N–O	Yin et al. (2019b)
	p-Nitrophenol	[$RuH_x$$MoO_{3-y}$(100)] = 2.5 g/L, $[PNP]_0$ = 1.5 mM, T = 25 °C, reaction time = 80 min, H_2, UV–Vis	0.063 min^{-1}	100%	Active centers, N–O	Yin et al. (2019a)
	Water-soluble aromatic amines Azo dyes	[g-C_3N_4/Fe_3O_4/p-RuNP] = 80 mg/L, $[AA]_0$ = 5.0 mg/L, pH = 7.0, reaction time = 8 min, UV–Vis	–	98%	$^{\cdot}OH$, $HO_2^{\cdot}$, hv	Sahoo and Patra (2020)

CV crystal violet, *CR* Congo red, *BP* Butylparaben, *DCF* Diclofenac, *PH* Phenol, *SA* Sulfanilamide, *RM, SMX Sulfamethoxazole,* MWCNTs Multiwall carbon nanotubes, *AMX* Amoxicillin, *4-CP* Chlorophenol, *TNW Titanate nanowires, TRA* Trazodone, *CTC* Chlortetracycline, *CP* Cyclophosphamide, *IF* Ifosfamide, *CF* Caffeine, *MO Titanate nanowires, PS* Persulfate, *TNT* Titanate nanotubes, *AA* Aromatic amines, *Vis Visible light*, *SSL* Simulated sunlight, *PAA* Peracetic acid, *COD* Chemical oxygen demand, *CP* 4-Chlorophenol, *MB* Methyl blue, *PNP p*-Nitrophenol, *LDH* Layered double hydroxides, *NDMA* N-nitrosodimethylamine, *CNT* carbon nanotube, *NP* nanoparticles, *OPD o*-phenylenediamine, *GO* Graphite oxide

[a]Catalyst loading normalized rate constants (L h^{-1} g_{cat}^{-1})

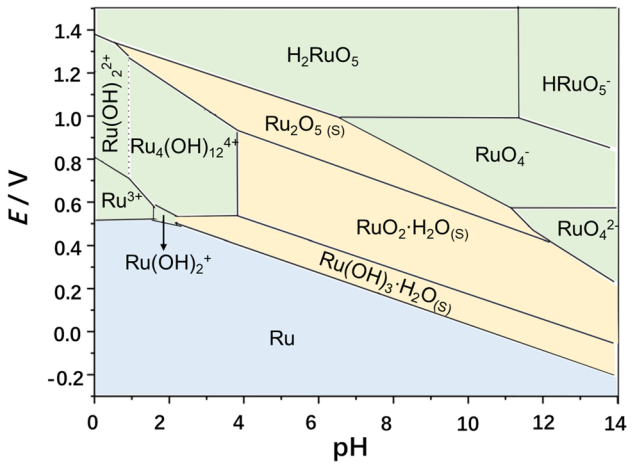

Fig. 1 Potential—pH diagrams for ruthenium compounds in the system Ru–H_2O, C^0_{Ru}= 10^{-4} mol/L. The equilibria were analyzed between chemical species in the solution and solid phase, considering only the electrode potentials of redox couples. At low potential, ruthenium was stable and existed in metallic phase. With the potential increased, ruthenium was oxidized to III at acidic media and also could be oxidized to IV at neutral and basic media. With the increase in the total concentration of ruthenium: **a** the areas of stability of $Ru(OH)_2^+$, $Ru(OH)_2^{2+}$, RuO_4^{2-}, RuO_4^- significantly narrow; **b** the thermodynamic stability areas of the solid phase $Ru(OH)_3{\bullet}H_2O_{(S)}$, $RuO_2{\bullet}H_2O_{(S)}$, and $Ru_2O_{5(S)}$ increase

$$NHCl_2 + H_2O \rightarrow NOH + 2H^+ + 2Cl^- \quad (4)$$

$$NH_2Cl + NOH \rightarrow N_2 + H^+ + Cl^- + H_2O \quad (5)$$

$$NHCl_2 + NOH \rightarrow N_2 + 2H^+ + 2Cl^- \quad (6)$$

$$NH_4^+ + 3HO^{\cdot} \xrightarrow{H_2N-NH_2} \frac{1}{2}N_2 + H^+ + 3H_2O \quad (7)$$

$$H_2O \rightarrow HO^{\cdot}(ads) + H^+ + e^- \quad (8)$$

$$HO^{\cdot}(ads) + Cl^- \rightarrow Cl^{\cdot} + OH^- \quad (9)$$

$$Cl^- \rightarrow Cl^{\cdot}(ads) + e^- \quad (10)$$

$$Cl^- + Cl^{\cdot} \rightarrow Cl_2(aq) + e^- \quad (11)$$

$$Cl_2 + H_2O \rightarrow HOCl + Cl^- + H^+ \quad (12)$$

$$HOCl \leftrightarrow H^+ + OCl^- \quad (13)$$

$$HO^{\cdot} + OCl^- \rightarrow ClO^{\cdot} + OH^- \quad (14)$$

$$Cl^{\cdot} + OCl^- \rightarrow Cl^- + ClO^{\cdot} \quad (15)$$

Photocatalytic oxidation

Ru-based nanocomposites have received considerable interest as photosensitizers and photocatalysts for water decontamination (Yin et al. 2019b; Akshatha et al. 2020; Osawa et al. 2020). Jiang et al. (2018) synthesized Ru-based complex@g-C_3N_4/TiO_2 hybrid composites using a solvothermal approach for the photocatalytic removal of methyl blue in water. Ru-modified g-C_3N_4/TiO_2 exhibited a twofold higher degradation of methyl blue (0.0336 min^{-1}) under visible light irradiation than bare g-C_3N_4/TiO_2 (0.0176 min^{-1}) (Table 1). Notably, the heterojunction in the hybrid composites enhances the separation performance of the photoexcited electrons and holes (Fig. 2). This was mainly attributed to the high visible light absorption and quantum efficiency of Ru-based complexes, which can be photosensitized to the RuC^{2+*} excited state. This species could efficiently transfer photogenerated electrons to the conduction band of g-C_3N_4, possibly promoting the conversion of dissolved oxygen to reactive oxidizing species.

Photocatalytic mechanisms were proposed with the involvement of superoxide radicals ($O_2^{\bullet-}$) and $^{\bullet}OH$, which could accomplish the efficient oxidation of methyl blue. Similar photocatalytic mechanisms have also been reported during the removal of caffeine and anticancer drugs, aromatic amines, and phenazopyridine over Ru-modified crystalline titanate nanowires (Osawa et al. 2019; Barrocas et al. 2019), g-C_3N_4/Fe_3O_4/porous Ru nanocatalyst (Sahoo and Patra 2020), and Ru-sensitized TiO_2 electrospun fibers (Boyer et al. 2016), respectively. Additionally, Ru-based metal complexes (including *tris*-(2,2′-bipyridine) Ru(II) chloride and *tris*-(1,10-phenanthroline) Ru(II) chloride) can be effectively photosensitized under solar light illumination to produce $^1O_2$ (Salazar-Rábago et al. 2016a). This reactive intermediate decomposed chlorotetracycline at a sevenfold reaction rate compared to direct photolysis. Notably, introducing humic acid inhibited the performance of Ru-based photosensitizers but facilitated the direct photolysis of the target antibiotic. The redox potentials of the Ru(IV)/Ru(III) (+0.77 V) and Ru(V)/Ru(IV) (1.22 V) pairs also contributed to the electron donor/acceptor-mediated surface charge transfer of the heterogeneous Ru-based photocatalysts. In a recent study, Yin et al. (2019a) reported the superior photocatalytic reduction of toxic *p*-nitrophenol (PNP) to *p*-aminophenol using plasmonic Ru/hydrogen molybdenum bronzes (Ru/H_xMoO_{3-y}) under visible light irradiation. The catalytically active sites were identified as surface-doped Ru nanoparticles, while H_xMoO_{3-y} acted as the electron-donor centers for N–O bond reduction. Furthermore, introducing additional oxidants, e.g., persulfate, could greatly promote

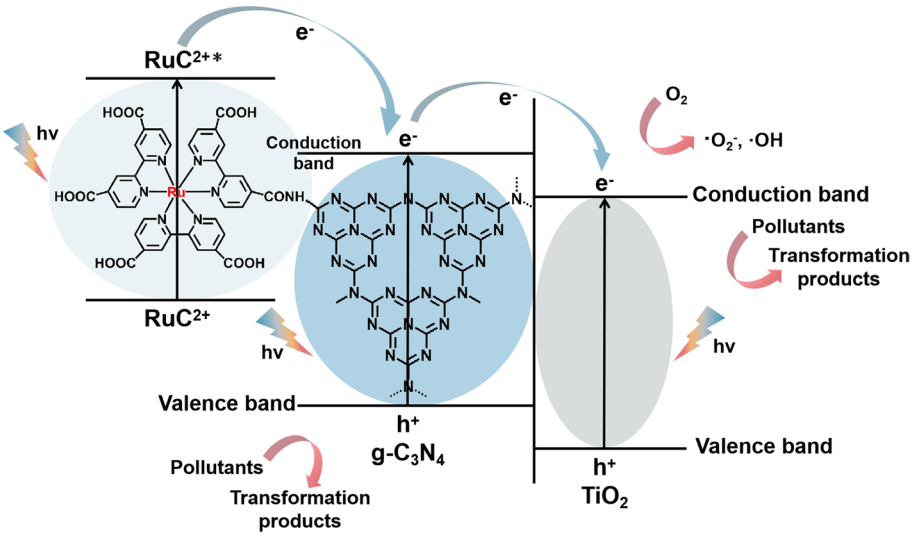

Fig. 2 Tentative photocatalytic oxidation mechanisms for methyl blue degradation using RuC@g-C_3N_4/TiO_2 hybrid. Reproduced with permission from reference (Copyright 2018, Elsevier). Several reactive species would generate for RuC@g-C_3N_4/TiO_2 hybrid through the reactions with the holes and electrons, which are considered involved in the actual oxidative and reductive reactions. The species are generally called reactive oxygen species including superoxide anion radical ($^{\bullet}O_2^-$), hydrogen peroxide (H_2O_2), singlet oxygen ($^1O_2$), and hydroxyl radical ($^{\bullet}OH$), which have enough strong reactivity to degrade almost all organic pollutants Jiang et al. (2018)

the decomposition of methyl orange and accomplish complete bacterial inactivation in visible light-activated tris(2,2′-bipbipyridyl(II) complex system (Subramanian et al. 2013).

Additionally, a combination of photocatalysis and electrochemical oxidation has been proposed as an efficient approach for the aqueous removal of different organic micropollutants (Moraes et al. 2016; García-Ramírez et al. 2021). Moraes et al. (2016) reported that the RuO_2-graphene electrode, in the absence of light and after 1 h, achieved a percentage of hormone degradation of 59.5%. However, the presence of light promoted a removal of 92.2% of 17β-estradiol after 1 h of photoelectrocatalytic treatment under pseudo-first-order kinetics. In a recent investigation, Ru/Ti/TiO_2 nanotubes were prepared and employed as a photoanode array for the photoelectrochemical removal of Terasil Blue dye under UV–vis light illumination (García-Ramírez et al. 2021). The ruthenium-doped TiO_2 nanotube array photoanodes showed a peak photocurrent and a saturation photocurrent upon their illumination with UV or visible light. In contrast, the undoped TiO_2 nanotubes only showed the saturation photocurrent, which was higher than that reached with the ruthenium-doped photoanodes using UV light. It was observed that Ru addition with 0.15 wt% significantly enhanced the dye removal to 98% and 55% in photoelectrochemical with UV and visible light, respectively, than the undoped TiO_2 (82% and 28%) after 2.0 h of treatment. This study suggests that Ru-based photoanodes can efficiently decompose organic contaminants using solar light as the ultraviolet–visible source. The application of a rather small bias (i.e., anodic) potential to the illuminated photoanode, which favors the spatial separation of both charge carriers, since the electrons are immediately transported to the cell cathode. Therefore, the combination of photocatalysis and electrocatalysis could lead to a larger accumulation of hydroxyl radicals and holes under visible light as compared to photocatalysis alone, thereby upgrading the oxidation of the organic contaminants.

Activation of inert oxidants for pollutant oxidation

Studies have increasingly suggested that Ru-based nanocomposites can be utilized as highly efficient activators of multiple oxidants (e.g., peracetic acid, oxone, and Mn(VII)) for catalytic pollutant removal (Sahoo and Patra 2018; Serra-Pérez et al. 2021; Zhang et al. 2015; Zhou et al. 2022). Detailed information on the catalytic performance in different oxidation systems is provided in Table 1, and the reactive species generated are illustrated in Fig. 3a. Sharma and his colleagues compared removal efficiency of sulfamethoxazole among several individual transition metals, i.e., Fe(II), Co(II), Mn(II), Cu(II), Ni(II), Fe(III), and Mn(III), and the results showed clearly that Ru(III) was the most effective peracetic acid activator to completely degrade sulfamethoxazole (Fig. 3b) (Li et al. 2021). Pan et al. (2021) found that RuO_2-rectorite exhibited complete Fenton-like oxidation of sulfanilamide at pH 3.5 via the transformation of H_2O_2–$^{\bullet}OH$. This composite also showed superior stability, high catalytic efficiency, and low Ru leaching during the recycling experiments (Fig. 4). Ru(III) was recently demonstrated to significantly activate peracetic acid to oxidize

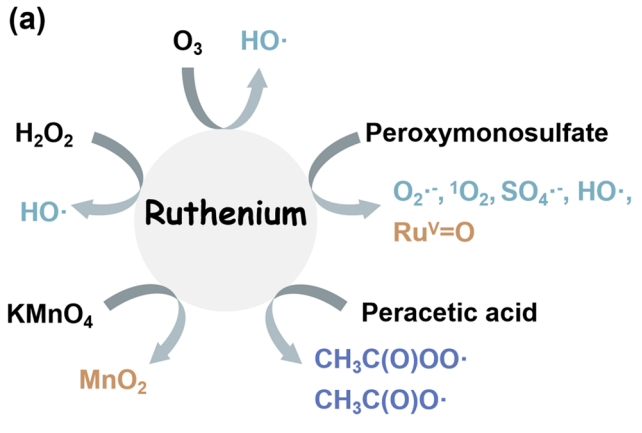

Fig. 3 **a** Possible mechanisms for activation of oxidants by supported ruthenium nanoparticles. **b** Degradation of sulfamethoxazole by peracetic acid activated by different metal ions, including Ru(III), Co(II), Fe(II), Fe(III), Mn(II), Mn(III), Ni(II), and Cu(II). (Experimental conditions: [sulfamethoxazole] = 10.0 μM, [peracetic acid] = 200.0 μM, [metal ions] = 100.0 μM, pH = 7.0 ± 0.1, 10.0 mM phosphate buffer, $T = 25 \pm 1$ °C.)

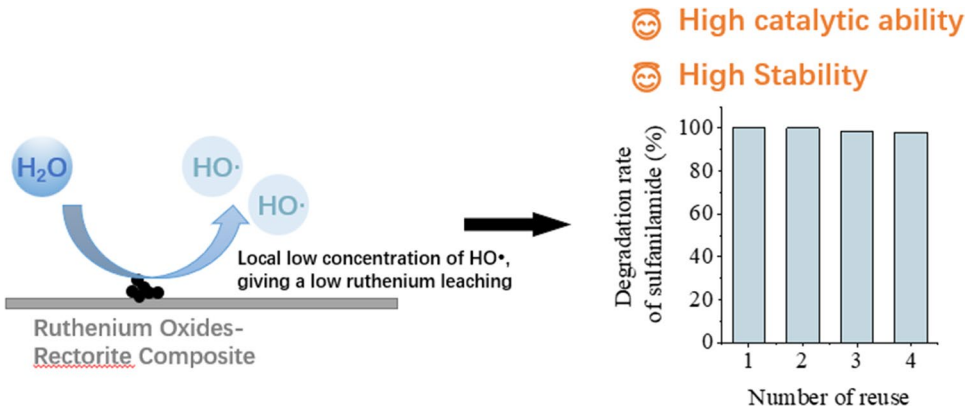

Fig. 4 Ruthenium oxide-rectorite composites applied in a heterogeneous Fenton-like system for efficient degradation of sulfanilamide. A high catalytic efficiency was observed on such composite and the degradation process conformed to pseudo-first-order kinetic correlation. The leaching amount of ruthenium was 0.30 μg/L in 5 h and ruthenium oxide-rectorite possessed excellent reusability as well

multiple organic micropollutants under neutral pH conditions, which was much better than other metal ions-peracetic acid systems (Li et al. 2021). The coexisting water constituents, e.g., chloride and carbonate ions, had little effect on the oxidizing performance of the Ru-based catalysts (Fig. 5a) (Li et al. 2021). Mechanistic insights were obtained using electron paramagnetic resonance analysis and quenching tests, revealing the dominance of acetyl(per)oxyl radicals in accelerated pollutant elimination. Similar phenomena were also reported in a heterogeneous peracetic acid activation system using RuO_2-modified multi-well carbon nanotubes, in which surface-bound Ru(III)/Ru(IV)-mediated electron transfer played a critical role in tuning radical generation (Qian et al. 2022). Furthermore, Ru-based composites (e.g., Ru/molecular sieves, Ru/TiO_2, and Ru/CeO_2) can greatly enhance the Mn(VII) oxidation of organic micropollutants in different water matrices (Zhang et al. 2013, 2014, 2015). The catalytic performance depended on the solution pH and catalyst dose (Fig. 5b, c) (Li et al. 2021). In particular, the surface-deposited Ru(III) functioned as an electron shuttle to modulate the Mn(VII) reactivity to form MnO_2, while the resultant higher-valence Ru(VI) and Ru(VII) facilitated micropollutant oxidation as the co-oxidants. Notably, these Ru-based nanoparticles exhibited excellent stability during Mn(VII) oxidation.

In terms of oxone activation, various Ru-based catalysts (e.g., RuO_2/Al_2O_3, RuO_2 nanosheets, Ru-doped C_3N_4) have been reported for the highly effective decomposition of micropollutants (Lim et al. 2019; Yan et al. 2022; Zhou et al. 2022). An initial attempt was made using activated carbon-supported RuO_2 catalysts to activate Oxone to eliminate phenol in water (Muhammad et al. 2012). Remarkably enhanced oxidation was obtained with 100% phenol abatement and 60% total organic carbon removal, which were dependent on multiple reaction conditions, e.g., catalyst dosage, phenol level, and oxone concentration. The mechanistic analysis demonstrated the dominant role of $SO_4^{\bullet-}$ from oxone activation for sustainable water decontamination, and the activation energy was calculated to be 61.4 kJ/mol. A similar conclusion was obtained for oxone activation using highly

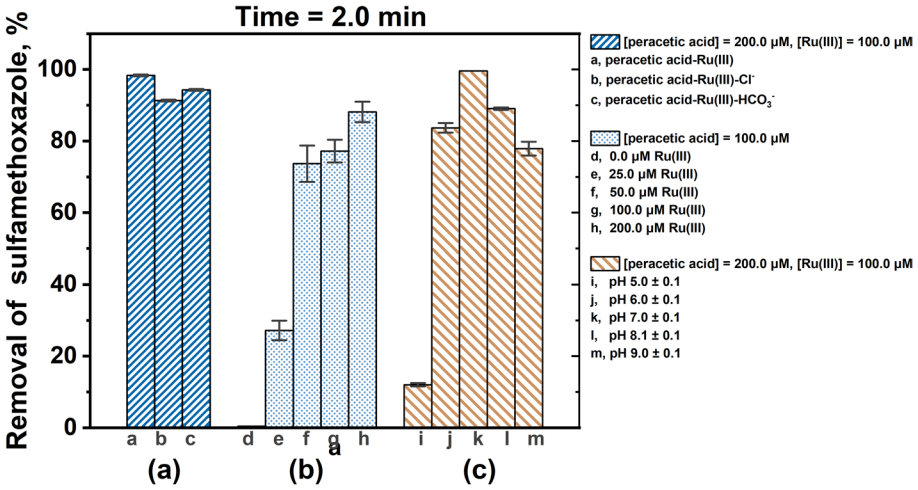

Fig. 5 **a** Effect of chloride (Cl^-) and bicarbonate (HCO_3^-) on the oxidation of sulfamethoxazole by peracetic acid − Ru(III). Experimental conditions: [sulfamethoxazole] = 10.0 μM, [peracetic acid] = 200.0 μM, [Ru(III)] = 100.0 μM, pH = 7.0 ± 0.1, 10.0 mM phosphate buffer, T = 25 ± 1 °C, [Cl^-] = 1.0 mM, [HCO_3^-] = 1.0 mM. **b** Effect of Ru(III) concentration, and **c** effect of pH on the degradation of sulfamethoxazole by the peracetic acid–Ru(III) oxidation process. Experimental conditions: [sulfamethoxazole] = 10.0 μM, [peracetic acid] = 25.0 − 200.0 μM, Ru(III) = 25.0 − 200.0 μM, pH = 7.0 ± 0.1 except (C), 10.0 mM phosphate buffer, and T = 25 ± 1 °C (Li et al. 2021)

stable two-dimensional RuO_2 nanosheets for the aqueous abatement of aromatic and non-aromatic compounds (Lim et al. 2019).

In addition to the radical-dominated mechanisms, Yan et al. (2022) and Zhou et al. (2022) reported non-radical-mediated diclofenac degradation and bacterial inactivation using Ru-C_3N_4 and Ru-layered double hydroxides, respectively. In particular, complete abatement of diclofenac was achieved within 10 min at pH 3.0–9.0 in the Ru-C_3N_4/Oxone system, which was much better than that in the other metal-C_3N_4/oxone systems. This nanocomposite also exhibited prominent catalytic stability with limited Ru leaching. The activation mechanisms were proposed to be initiated by electron defect transfer between Ru and pyridine nitrogen. This is followed by the formation of $O_2^{\bullet-}$, which is rapidly converted to $^1O_2$ for pollutant removal. Product analysis and in silico toxicity prediction confirmed that the aquatic toxicity of the oxidized intermediates was lower than the parent compound. More recently, the homogeneous oxone activation by aqueous Ru(III) presented a high oxidation performance for different micropollutants mediated by the high-valent $Ru^V=O$ intermediate (Zong et al. 2021). This newly detected Ru-based species mainly attacked the electron-rich moiety of the organic compounds, giving a higher oxidative selectivity than the radical species. Taken together, multiple reactive oxidizing species were involved in the Ru-driven oxone oxidation system, including $^{\bullet}OH$, $SO_4^{\bullet-}$, $^1O_2$, and $Ru^V=O$ intermediates. More in-depth investigations are eagerly pursued to clarify the underlying mechanisms of the chemical generation and modulation of reactive species in different Ru-based oxidation systems.

Catalytic reduction

Hydrogen-assisted reduction

Hydrogen (H_2)-assisted decontamination of oxyanion (AO_x^-) pollutants in wastewater on Ru-based catalysts has been widely reported, e.g., NO_3^-, ClO_3^-, BrO_3^-, and ClO_4^- (Huo et al. 2017). Those toxic oxyanions are ubiquitous drinking water contaminants originating from both anthropogenic and natural sources, or are generated during water treatment processes (e.g., chlorination, ozonation, desalination, and electrochemical treatment) (Chen et al. 2017). These ions target multiple organs and can have carcinogenic, mutagenic, and/or endocrine disrupting properties. Catalytic reduction by H_2 was a charming technology to convert oxyanions into less toxic or innocuous end products (e.g., Br^-, Cl^- and N_2), contributing to more sustainable drinking water treatment processes. There are two main pathways of oxyanion reduction by H_2 on the Ru-based catalyst, including direct interaction with the hydrogenated metal nanoparticles (reactions 16–19), and the reaction between AO_x^- and spilled over atomic hydrogen at catalyst support surface away from the hydrogenated metal nanoparticles (reactions 20 and 21) (Chen et al. 2017) (Fig. 6),

$$H_2 + {}^*M \rightarrow 2[H]_{ads} - M \quad (16)$$

$$AO_x^- + {}^*M \leftrightarrow (AO_x^-)_{ads} - M \quad (17)$$

$$(AO_x^-)_{ads} - M + 2[H]_{ads} - M \rightarrow (AO_{x-1}^-)_{ads} - M + H_2O \quad (18)$$

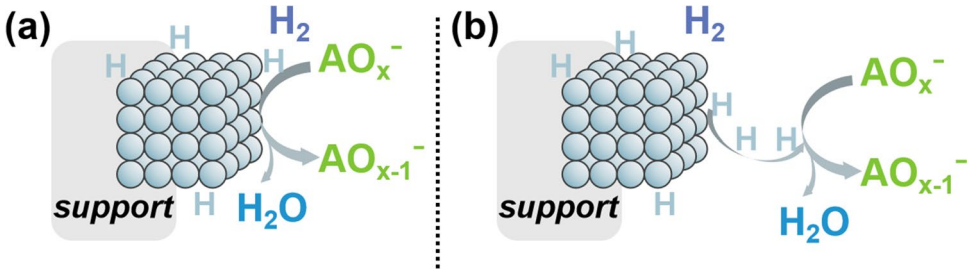

Fig. 6 **a** The proposed reductive mechanisms of oxyanion substrates (AO_x^-) reduction requiring direct interaction with the Ru nanoparticles; **b** the reaction between AO_x^- and spilled over atomic hydrogen at the catalyst support surface away from Ru nanoparticles. Modified with permission from Chen et al. (2017) (Copyright 2017, Elsevier)

$$(AO^-_{x-1})_{ads} - M \leftrightarrow AO^-_{x-1} + {}^*M \quad (19)$$

$$[H]_{ads} - M + {}^*Support \rightarrow {}^*M + [H]_{ads} - Support \quad (20)$$

$$2[H]_{ads} - Support + AO^-_x \rightarrow AO^-_{x-1} + {}^*Support + H_2O \quad (21)$$

where M is the metallic Ru surface and $[H]_{ads} - M$ is the chemisorbed hydrogen.

The kinetics of oxyanion reduction were highly dependent on the molecular structure of the components. Reduction of the four oxyanion contaminants with a broad range of chemical reactivity ($BrO_3^- \gg ClO_3^- > NO_3^- \gg ClO_4^-$) was observed (Chen et al. 2017). In addition, ClO_3^- and NO_3^- reduction on Ru nanoparticles under circumneutral pH conditions was independent of pH (Chen et al. 2017), but pH-sensitive activity was observed for BrO_3^- reduction, and a significant decay of catalytic activity was observed as the solution pH increased (Fan et al. 2019). BrO_3^- reduction on Ru was rather efficient if H_2 gas was sufficient (~ 100 mL min^{-1}), and the reaction followed pseudo-first-order kinetics, which revealed that the adsorption of BrO_3^- ions onto the Ru surface was the rate-determining step. The zeta potential of the Ru-based catalyst decreased with an increase in the solution pH. In the acidic medium, the functional groups on the surface of the Ru-based catalyst were protonated, causing an electrostatic attractive interaction between BrO_3^- and Ru-based catalysts, which was beneficial for promoting BrO_3^- reduction. In contrast, the Ru-based catalyst was negatively charged at a higher pH, and the electrostatic repulsion between BrO_3^- and Ru-based catalysts suppressed the adsorption reduction of BrO_3^-. For the ClO_3^- and NO_3^-, their kinetic rates on Ru were so low that their activities were insensitive to the solution pH (Chen et al. 2017).

Electroreduction

The electrochemical reduction has emerged as a promising alternative with outstanding safety advantages that can avoid H_2 storage and transportation. In a recent study, Sun et al. (2022) reported the application of a Ru/carbon nanotube catalyst for the highly efficient electroreduction of *N*-nitrosodimethylamine, a common carcinogenic and genotoxic compound in water. This Ru-based composite presented a higher catalytic performance (793.3 μmol L^{-1} g_{cat}^{-1} h^{-1}) for *N*-nitrosodimethylamine reduction than the other metal-doped carbon nanotube did (i.e., Rh/carbon nanotube, 471.0 μmol L^{-1} g_{cat}^{-1} h^{-1}; Pd/carbon nanotube, 313.8 μmol L^{-1} g_{cat}^{-1} h^{-1}; Pt/carbon nanotube, 152.3 μmol L^{-1} g_{cat}^{-1} h^{-1}) (Table 1). The combined quenching tests and reactive species identification suggested that direct electron reduction on the electrode surface and indirect atomic hydrogen (H^*)-triggered reduction were the two dominant reaction patterns for the conversion of nitrosodimethylamine to dimethylamine and ammonia (Fig. 7). This Ru-driven electrocatalytic system could also possess a superior reductive efficiency for different dialkyl *N*-nitroamines, suggesting its universality. Recycling experiments demonstrated the excellent stability of the Ru/carbon nanotube electrocatalyst for *N*-nitrosodimethylamine reduction. Ru was proved to strongly adsorb hydrogen, which was further formed as an active H^* via the Volmer step (Xu et al. 2018). Electrochemical hydrogenation is the main mechanism occurring on Ru during the electroreduction of aquatic pollutants (Chen et al. 2017; Zhu et al. 2021a). In the reaction system, electrochemical hydrogenation chemisorbed hydrogen is generated at the cathode surface through the reduction of water (Eq. 22).

$$2H_2O + 2e^- + M \rightarrow 2[H]_{ads} - M + 2OH^- \quad (22)$$

It should be noted that during electrochemical hydrogenation, the hydrogen evolution reaction, via the Heyrovsky or Tafel step (reactions 23 and 24), inevitably competes with the reduction of pollutants (Moya et al. 2020), if too many H^* are accumulated on the Ru surface. Hence, the rate of water reduction should be lower than the pollutants'

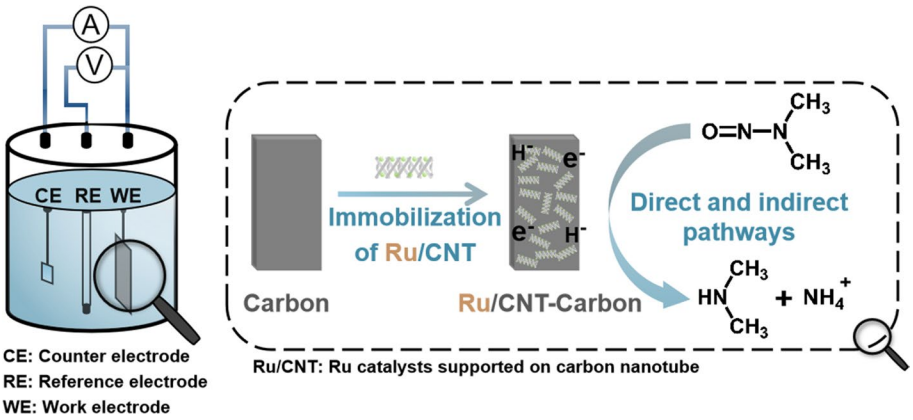

Fig. 7 Mechanistic illustrations of highly effective electrocatalytic reduction of nitrosodimethylamine on Ru/carbon nanotube catalyst. The electrocatalytic reduction of nitrosodimethylamine is accomplished by both direct electron reduction and atomic H*-mediated indirect reduction pathways. Nitrosodimethylamine would be finally reduced to dimethylamine and ammonia. The reduction efficiency of nitrosodimethylamine strongly relies on cathode potential, initial concentration, and solution pH. Modified with permission from Sun et al. (2022) (Copyright 2022, Elsevier)

hydrogenation step. Otherwise, the evolved H_2 could form a layer covering the electrode surface and limit the mass transfer of pollutants to the active sites. As a result, the hydrogenation of pollutants was counteracted. Sun et al. (2022) found that an enhanced *N*-nitrosodimethylamine removal with potential increasing from −0.7 to −0.9 V versus saturated calomel electrode was obtained and attributed to the more effective generation of active H^* and provision of reductive electrons (e^-) at more negative potentials; however, further increasing potential from −0.9 to −1.1 V *versus* saturated calomel electrode did not bring in significant enhancement of nitrosodimethylamine reduction, since the H_2 evolution gradually prevails on the electrode via recombination of H^* to form H_2 by the Heyrovsky or Tafel routes at lower potentials. Remarkable H_2 evolution on the electrode leads to a decrease in the number of catalytically active sites and prohibits the migration of active electrons and pollutants at the electrode interface.

$$[H]_{ads} - M + H_2O + M + e^- \rightarrow H_2 + OH^- \quad (23)$$

$$[H]_{ads} - M + [H]_{ads} - M \leftrightarrow H_2 \quad (24)$$

Other catalytic reductions

Pollutants could also be efficiently eliminated over Ru-based catalysts using $NaBH_4$ (Zhao et al. 2018; Zaoui et al. 2021) or N_2H_4 (Rambabu et al. 2015; Zhao et al. 2017b) as reductants. Veerakumar et al. (2015) applied $NaBH_4$ as a hydrogen donor to reduce *p*-nitroaniline over Ru nanoparticle-modified 3D mesoporous carbon and obtained a high apparent kinetic rate of *p*-nitroaniline reduction around 0.19 s^{-1}. Zhao et al. (2017a) found that Ru nanoparticles showed superior size-dependent catalytic performance with the best kinetic rate constant of 1.52 min^{-1} during the catalytic reduction of nitroaromatic compounds and azo dyes. The apparent kinetic rate of Ru nanoparticles with a small size (2.6–8.2 nm) could far surpass the catalyst with a large size of 8.2–51.4 nm. $NaBH_4$, which features strong reducibility, provided the possibility of reducing nitroaromatic compounds to amines (Chu and Su 2014). However, this process is kinetically restricted in the absence of nanocatalysts and proceeds slowly. Here, the presence of Ru nanoparticles nanocatalysts lowered the activation energy and accelerated electron transfer from $NaBH_4$ to the probes. Electrons transferred from BH_4^- provided electrons and protons to the probes adsorbed on the surface of the Ru-based catalyst (Chauhan and Srivastava 2020). The adsorption of the probes was driven by chemical interactions (chemisorption) between the particle surface and probes. Finally, the end product was formed, followed by the desorption of the product from the Ru surfaces and reactivation of the catalytic system. Ru nanoparticles also exhibited superior catalytic performances in comparison to Pt nanoparticles and Ir nanoparticles at ambient temperatures. The kinetic rate constant of Ru nanoparticles was almost 64-fold and 12-fold higher than that of Ir nanoparticles and Pt nanoparticles.

Environmental impact

The United Nations Sustainable Development Goals provide "a blueprint for peace and prosperity for people and the planet," set out in the 2030 Agenda for Sustainable Development and adopted by all UN member states in 2015. The

Ru-driven environmental catalysis for water decontamination would substantially minimize illnesses from hazardous chemicals and air, water, and soil pollution and contamination, which would help achieve the goals of "Good Health and Well-Being." On the other hand, the Ru-driven advanced oxidation and reduction technology could improve water quality by reducing pollution, eliminating dumping, minimizing the release of hazardous chemicals and materials, halving the proportion of untreated wastewater, and substantially increasing recycling and safe reuse globally. These features promote the achievement of the goals of "Clean Water and Sanitation" by 2030. The land-based activities were closely related to the ocean ecological system. Efficient elimination of the refractory organic and inorganic compounds prior to their entrance to the ocean would prevent and significantly reduce marine pollution.

Therefore, application of Ru-driven environmental catalysis for sustainable water decontamination is considered an effective and environmentally friendly process for degradation of the toxic and bio-recalcitrant pollutants. Prior to scaling up this catalytic system for future practical applications, some obstacles need to be addressed. The complexity of the matrix of the wastewater is one of the challenges of implementing Ru-based catalysts in the treatment of real wastewater. The presence of various organic and inorganic compounds might severely poison the catalytic sites and in turn decrease the removal efficiency. For example, reduced sulfur compounds (RSCs), coming partly from microbial anaerobic reaction or contained in the natural organic matter, have shown a poisoning effect on the catalytic ability by the adsorption of sulfur and the formation of Ru sulfide on the catalyst surface. In that case, the hydrogen adsorption on Ru is hindered, and the mobility of the hydrogen atoms located on the catalyst surface is reduced. On the other hand, the presence of organic suspended solids in the wastewater would inevitably limit the photocatalytic efficiency so some pretreatments should be implemented to remove the suspended matters. In addition, the low conductivity of real wastewater (compared to synthetic effluents) is often a major bottleneck for the development of electrochemical technologies for environmental remediation. Since all the Ru species are toxic, especially the RuO_2, the stability of catalysts is critical for the safety of treatment effluent. Finally, strides should be made on preparing catalysts, which should be cost-effective and environmentally friendly.

Conclusion

With increasingly serious water pollution, a simple, non-hazardous, low energy input, and efficient treatment process is highly desirable for the degradation of micropollutants, pathogenic microorganisms, oxyanions, and nitrosamines in drinking water and wastewater treatment. Ru, as the cheapest noble metal as catalysts, has been proven to have high activity for the elimination of pollutants by oxidation processes carried out by oxone, $^{\bullet}OH$, $^1O_2$ formation, and high-valence Ru, or by reduction processes via H^* attack. To promote further practical application of Ru-based materials in water treatment, three efforts may be made:

(1) Control of Ru leaching

Ru composites are toxic to many aquatic organisms (Kruszyna et al. 1980; Mello-Andrade et al. 2018). Ru nanocatalysts are suggested to be well deposited on suitable substrates where Ru could be well anchored so that less leakage of Ru species could be achieved. Metal alloys are composed of different atoms, unlike pure metals, where the atoms are all the same. This makes it harder for atoms to move around in metal alloys, leading to alloys that are typically much more durable than pure metals. Hence, Ru-based alloys are expected to achieve better durability during catalysis.

(2) Selective catalysis

Oxidation process: Ru-driven environmental catalysis can generate multiple reactive oxidizing species such as $^{\bullet}OH$, $SO_4^{\bullet-}$, $^1O_2$, and $Ru^V=O$ intermediates. Among them, the less selective $^{\bullet}OH$ and $SO_4^{\bullet-}$ species could also react with the background water constituents (e.g., nitrate, chloride, and dissolved organic matter), causing unnecessary oxidant consumption and the production of toxic byproducts. Comparatively, $^1O_2$ and $Ru^V=O$ species are recognized as selective oxidants that preferentially attack the target micropollutants and pathogenic bacteria for water decontamination. Therefore, another research frontier would be tuning the generation of selective oxidizing species in Ru-catalyzed chemical systems to achieve more environmentally friendly and efficient water remediation.

Reduction process: hydrogenation is the main mechanism of pollutant reduction over Ru-based catalysts. It is highly important to avoid the hydrogen evolution reaction (H* coupling process) to improve energy efficiency. The hydrogenation activity was affected by the complexity of the matrix of the wastewater effluent. The presence of various organic and inorganic compounds may severely hinder the reduction of the target compound and, in turn, decrease the removal efficiency. In addition, the low conductivity of real wastewater compared to synthetic effluents is often a major bottleneck for the development of electrochemical reduction technologies for environmental remediation.

(3) Reactivity modulation

The rational design of catalysts is of great importance for promoting the catalytic activity of Ru for pollutant decontamination. Several strategies can be

used to improve the catalytic activities: (1) precisely tuning the catalysts' crystalline facets. Numerous studies have reported that pollutant elimination is a facet-dependent reaction (Chai et al. 2017; Jiang et al. 2020; Lou et al. 2022); (2) defect engineering. The defective sites are not only more likely to exhibit selective adsorption of target pollutants from complex matrix but also have a higher ability of radicals and H^* formation to attack the pollutants (Liu et al. 2018; Shen et al. 2020), and (3) bimetallic surfaces and alloys (Koper 2004). The enhanced catalytic activity of bimetallic surfaces in comparison to monometallic surfaces is usually ascribed to two effects: the bifunctional effect, in which the unique catalytic properties of each of the elements in the alloy combine in a synergetic fashion to yield a surface that is more active than each of the elements alone, and the ligand or electronic effect, in which one of the elements alters the electronic properties of the other to yield a more active catalytic surface; (4) other approaches such as tuning the nanoparticle or nanocluster' size (Nutt et al. 2005; Zhao et al. 2017a) and selective suitable support to have a support effect (Comotti et al. 2006).

Acknowledgements The authors want to thank the support of the President Research Funds from Xiamen University (20720210081).

Declarations

Conflict of interest The authors declared no conflict of interest.

References

Akshatha S, Sreenivasa S, Kumar KY et al (2020) Rutile, mesoporous ruthenium oxide decorated graphene oxide as an efficient visible light driven photocatalyst for hydrogen evolution reaction and organic pollutant degradation. Mater Sci Semicond Process 116:105156. https://doi.org/10.1016/j.mssp.2020.105156

Anbia M, Rezaie M (2016) Synthesis of supported ruthenium catalyst for phenol degradation in the presence of peroxymonosulfate. Water Air Soil Pollut 227:349. https://doi.org/10.1007/s11270-016-3047-0

Anbia M, Rezaie M (2017) Generation of sulfate radicals by supported ruthenium catalyst for phenol oxidation in water. Res Chem Intermed 43:245–257. https://doi.org/10.1007/s11164-016-2618-4

Angerani S, Winssinger N (2019) Visible light photoredox catalysis using ruthenium complexes in chemical biology. Chem Eur J 25:6661–6672. https://doi.org/10.1002/chem.201806024

Axet MR, Philippot K (2020) Catalysis with colloidal ruthenium nanoparticles. Chem Rev 120:1085–1145. https://doi.org/10.1021/acs.chemrev.9b00434

Bae SY, Mahmood J, Jeon IY, Baek JB (2020) Recent advances in ruthenium-based electrocatalysts for the hydrogen evolution reaction. Nanoscale Horiz 5:43–56. https://doi.org/10.1039/C9NH00485H

Barrocas BT, Oliveira MC, Nogueira HIS et al (2019) Ruthenium-modified titanate nanowires for the photocatalytic oxidative removal of organic pollutants from water. ACS Appl Nano Mater 2:1341–1349. https://doi.org/10.1021/acsanm.8b02215

Barrocas B, Conceição Oliveira M, Nogueira HIS et al (2020) A comparative study on emergent pollutants photo-assisted degradation using ruthenium modified titanate nanotubes and nanowires as catalysts. J Environ Sci 92:38–51. https://doi.org/10.1016/j.jes.2020.01.027

Biard PF, Werghi B, Soutrel I et al (2016) Efficient catalytic ozonation by ruthenium nanoparticles supported on SiO_2 or TiO_2: towards the use of a non-woven fiber paper as original support. Chem Eng J 289:374–381. https://doi.org/10.1016/j.cej.2015.12.051

Boyer SM, Liu J, Zhang S et al (2016) The role of ruthenium photosensitizers in the degradation of phenazopyridine with TiO_2 electrospun fibers. J Photochem Photobiol A Chem 329:46–53. https://doi.org/10.1016/j.jphotochem.2016.06.007

Cao GJ, Jiang X, Zhang H et al (2017) Mimicking horseradish peroxidase and oxidase using ruthenium nanomaterials. RSC Adv 7:52210–52217. https://doi.org/10.1039/c7ra10370k

Chai S, Wang Y, Zhang YN et al (2017) Selective electrocatalytic degradation of odorous mercaptans derived from s-au bond recongnition on a dendritic gold/boron-doped diamond composite electrode. Environ Sci Technol 51:8067–8076. https://doi.org/10.1021/acs.est.7b00393

Chauhan R, Srivastava VC (2020) Electrochemical denitrification of highly contaminated actual nitrate wastewater by Ti/RuO_2 anode and iron cathode. Chem Eng J 386:122065. https://doi.org/10.1016/j.cej.2019.122065

Chauhan R, Srivastava VC, Hiwarkar AD (2016) Electrochemical mineralization of chlorophenol by ruthenium oxide coated titanium electrode. J Taiwan Inst Chem Eng 69:106–117. https://doi.org/10.1016/j.jtice.2016.10.016

Chen X, Huo X, Liu J et al (2017) Exploring beyond palladium: catalytic reduction of aqueous oxyanion pollutants with alternative platinum group metals and new mechanistic implications. Chem Eng J 313:745–752. https://doi.org/10.1016/j.cej.2016.12.058

Chu C, Su Z (2014) Facile synthesis of AuPt alloy nanoparticles in polyelectrolyte multilayers with enhanced catalytic activity for reduction of 4-nitrophenol. Langmuir 30:15345–15350. https://doi.org/10.1021/la5042019

Chung LH, Yeung CF, Wong CY (2020) Ruthenium-induced cyclization of heteroatom-functionalized alkynes: progress, challenges and perspectives. Chem Eur J 26:6102–6112. https://doi.org/10.1002/chem.201905506

Comotti M, Li WC, Spliethoff B, Schüth F (2006) Support effect in high activity gold catalysts for CO oxidation. J Am Chem Soc 128:917–924. https://doi.org/10.1021/ja0561441

Fan C, Chen N, Feng C et al (2019) Enhanced performance and mechanism of bromate removal in aqueous solution by ruthenium oxide modified biochar (RuO_2/BC). Colloids Surf A Physicochem Eng Asp 572:27–36. https://doi.org/10.1016/j.colsurfa.2019.03.080

García-Ramírez P, Ramírez-Morales E, Solis Cortazar JC et al (2021) Influence of ruthenium doping on UV- and visible-light photoelectrocatalytic color removal from dye solutions using a TiO_2 nanotube array photoanode. Chemosphere 267:128925. https://doi.org/10.1016/j.chemosphere.2020.128925

Hemraj-Benny T, Tobar N, Carrero N et al (2018) Microwave-assisted synthesis of single-walled carbon nanotube-supported ruthenium nanoparticles for the catalytic degradation of Congo red dye. Mater Chem Phys 216:72–81. https://doi.org/10.1016/j.matchemphys.2018.05.081

Hodges BC, Cates EL, Kim JH (2018) Challenges and prospects of advanced oxidation water treatment processes using catalytic nanomaterials. Nat Nanotechnol 13:642–650. https://doi.org/10.1038/s41565-018-0216-x

Huo X, Van Hoomissen DJ, Liu J et al (2017) Hydrogenation of aqueous nitrate and nitrite with ruthenium catalysts. Appl Catal B 211:188–198. https://doi.org/10.1016/j.apcatb.2017.04.045

Huo X, Liu J, Strathmann TJ (2018) Ruthenium catalysts for the reduction of N-nitrosamine water contaminants. Environ Sci Technol 52:4235–4243. https://doi.org/10.1021/acs.est.7b05834

Izzudin NM, Jalil AA, Aziz FFA et al (2021) Simultaneous remediation of hexavalent chromium and organic pollutants in wastewater using period 4 transition metal oxide-based photocatalysts: a review. Environ Chem Lett 19:4489–4517. https://doi.org/10.1007/s10311-021-01272-1

Jiang G, Geng K, Wu Y et al (2018) High photocatalytic performance of ruthenium complexes sensitizing g-C_3N_4/TiO_2 hybrid in visible light irradiation. Appl Catal B 227:366–375. https://doi.org/10.1016/j.apcatb.2018.01.034

Jiang G, Li X, Shen Y et al (2020) Mechanistic insight into the electrocatalytic hydrodechlorination reaction on palladium by a facet effect study. J Catal 391:414–423. https://doi.org/10.1016/j.jcat.2020.09.008

Koper MTM (2004) Electrocatalysis on bimetallic and alloy surfaces. Surf Sci 548:1–3. https://doi.org/10.1016/j.susc.2003.10.045

Kruszyna H, Kruszyna R, Hurst J, Smith RP (1980) Toxicology and pharmacology of some ruthenium compounds: vascular smooth muscle relaxation by nitrosyl derivatives of ruthenium and iridium. J Toxicol Environ Health 6:757–773. https://doi.org/10.1080/15287398009529895

Kumar S, Singh S, Srivastava VC (2015) Electro-oxidation of nitrophenol by ruthenium oxide coated titanium electrode: parametric, kinetic and mechanistic study. Chem Eng J 263:135–143. https://doi.org/10.1016/j.cej.2014.11.051

Kümmerer K, Dionysiou DD, Olsson O, Fatta-Kassinos D (2018) A path to clean water. Science 361:222–224. https://doi.org/10.1126/science.aau2405

León I, Gomes H, Sepúlveda-Guzmán S et al (2021) Electro-oxidation of amoxicillin using titanium electrodes electrophoretically coated by iridium or ruthenium with tantalum oxides. J Chem Technol and Biotechnol 96:622–629. https://doi.org/10.1002/jctb.6575

Li R, Manoli K, Kim J et al (2021) Peracetic acid-ruthenium(III) oxidation process for the degradation of micropollutants in water. Environ Sci Technol 55:9150–9160. https://doi.org/10.1021/acs.est.0c06676

Lim J, Lee JM, Kim C et al (2019) Two-dimensional RuO_2 nanosheets as robust catalysts for peroxymonosulfate activation. Environ Sci Nano 6:2084–2093. https://doi.org/10.1039/c9en00500e

Liu R, Zhao H, Zhao X et al (2018) Defect sites in ultrathin pd nanowires facilitate the highly efficient electrochemical hydrodechlorination of pollutants by H^*_{ads}. Environ Sci Technol 52:9992–10002. https://doi.org/10.1021/acs.est.8b02740

Lou YY, Xiao C, Fang J et al (2022) High activity of step sites on Pd nanocatalysts in electrocatalytic dechlorination. Phys Chem Chem Phys 24:3896–3904. https://doi.org/10.1039/d1cp04975e

Majumdar D, Maiyalagan T, Jiang Z (2019) Recent progress in ruthenium oxide-based composites for supercapacitor applications. ChemElectroChem 6:4343–4372. https://doi.org/10.1002/celc.201900668

Mello-Andrade F, Cardoso CG et al (2018) Acute toxic effects of ruthenium (II)/amino acid/diphosphine complexes on Swiss mice and zebrafish embryos. Biomed Pharmacother 107:1082–1092. https://doi.org/10.1016/j.biopha.2018.08.051

Moraes FC, Gorup LF, Rocha RS et al (2016) Photoelectrochemical removal of 17β-estradiol using a RuO_2-graphene electrode. Chemosphere 162:99–104. https://doi.org/10.1016/j.chemosphere.2016.07.070

Moya A, Creus J, Romero N et al (2020) Organocatalyticvs.Ru-based electrochemical hydrogenation of nitrobenzene in competition with the hydrogen evolution reaction. Dalton Trans 49:6446–6456. https://doi.org/10.1039/d0dt01075h

Muhammad S, Shukla PR, Tadé MO, Wang S (2012) Heterogeneous activation of peroxymonosulphate by supported ruthenium catalysts for phenol degradation in water. J Hazard Mater 215–216:183–190. https://doi.org/10.1016/j.jhazmat.2012.02.045

Mutalib AAA, Jaafar NF (2022) Electrogeneration of active photocatalysts for wastewater remediation: a review. Environ Chem Lett 21:981–1003. https://doi.org/10.1007/s10311-022-01534-6

Nutt MO, Hughes JB, Wong MS (2005) Designing Pd-on-Au bimetallic nanoparticle catalysts for trichloroethene hydrodechlorination. Environ Sci Technol 39:1346–1353. https://doi.org/10.1021/es048560b

Osawa RA, Barrocas BT, Monteiro OC et al (2019) Photocatalytic degradation of cyclophosphamide and ifosfamide: Effects of wastewater matrix, transformation products and in silico toxicity prediction. Sci Total Environ 692:503–510. https://doi.org/10.1016/j.scitotenv.2019.07.247

Osawa RA, Monteiro OC, Oliveira MC, Florêncio MH (2020) Comparative study on photocatalytic degradation of the antidepressant trazodone using (Co, Fe and Ru) doped titanate nanowires: kinetics, transformation products and in silico toxicity assessment. Chemosphere 259:127486. https://doi.org/10.1016/j.chemosphere.2020.127486

Pan F, Yang J, Cai J, Liu L (2021) Heterogeneous Fenton-like oxidative degradation of sulfanilamide catalyzed by RuO_2-rectorite composite. Res Chem Intermed 47:4595–4611. https://doi.org/10.1007/s11164-021-04547-y

Peil S, Gutiérrez González A, Leutzsch M, Fürstner A (2022) C–H insertion via ruthenium catalyzed gem-hydrogenation of 1,3-enynes. J Am Chem Soc 144:4158–4167. https://doi.org/10.1021/jacs.1c13446

Peng X, Jiang Y, Chen Z et al (2023) Recycling municipal, agricultural and industrial waste into energy, fertilizers, food and construction materials, and economic feasibility: a review. Environ Chem Lett 21:765–801. https://doi.org/10.1007/s10311-022-01551-5

Qian Y, Huang J, Chen J et al (2022) Activation of peracetic acid by RuO_2/MWCNTs to degrade sulfamethoxazole at neutral condition. Chem Eng J 431:134217. https://doi.org/10.1016/j.cej.2021.134217

Rambabu D, Pradeep CP, Pooja DA (2015) Self-assembled material of palladium nanoparticles and a thiacalix[4]arene Cd(II) complex as an efficient catalyst for nitro-phenol reduction. New J Chem 39:8130–8135. https://doi.org/10.1039/c5nj01304f

Ray R, Hazari AS, Lahiri GK, Maiti D (2018) Ruthenium-catalyzed aerobic oxidation of amines. Chem Asian J 13:2138–2148. https://doi.org/10.1002/asia.201701748

Sahoo A, Patra S (2018) A combined process for the degradation of azo-dyes and efficient removal of aromatic amines using porous silicon supported porous ruthenium nanocatalyst. ACS Appl Nano Mater 1:5169–5178. https://doi.org/10.1021/acsanm.8b01152

Sahoo A, Patra S (2020) A magnetically separable and recyclable g-C_3N_4/Fe_3O_4/porous ruthenium nanocatalyst for the photocatalytic degradation of water-soluble aromatic amines and azo dyes. RSC Adv 10:6043–6051. https://doi.org/10.1039/c9ra08631e

Salazar-Rábago JJ, Sánchez-Polo M, Rivera-Utrilla J et al (2016a) Role of $^1[O_2]^*$ in chlortetracycline degradation by solar radiation assisted by ruthenium metal complexes. Chem Eng J 284:896–904. https://doi.org/10.1016/j.cej.2015.09.010

Salazar-Rábago JJ, Sánchez-Polo M, Rivera-Utrilla J et al (2016b) Organic xerogels doped with Tris(2,2′-bipyridine) ruthenium(II) as hydroxyl radical promoters: synthesis, characterization, and photoactivity. Chem Eng J 306:289–297. https://doi.org/10.1016/j.cej.2016.07.053

Sanz-Navarro S, Mon M, Doménech-Carbó A et al (2022) Parts–per–million of ruthenium catalyze the selective chain–walking reaction of

terminal alkenes. Nat Commun 13:2831. https://doi.org/10.1038/s41467-022-30320-9
Serra-Pérez E, Álvarez-Torrellas S, Ismael Águeda V et al (2021) Effective removal of naproxen from aqueous solutions by CWAO process using noble metals supported on carbon nanospheres catalysts. Sep Purif Technol 259:118084. https://doi.org/10.1016/j.seppur.2020.118084
Shen X, Xiao F, Zhao H et al (2020) In situ-formed pdfe nanoalloy and carbon defects in cathode for synergic reduction-oxidation of chlorinated pollutants in electro-fenton process. Environ Sci Technol 54:4564–4572. https://doi.org/10.1021/acs.est.9b05896
Silva MI, Burrows HD, Formosinho SJ et al (2007) Photocatalytic degradation of chlorophenols using $Ru(bby)_3^{2+}/S_2O_8^{2-}$. Environ Chem Lett 5:143–149. https://doi.org/10.1007/s10311-007-0096-z
Su Y, Muller KR, Yoshihara-Saint H et al (2021) Nitrate removal in an electrically charged granular-activated carbon column. Environ Sci Technol 55:16597–16606. https://doi.org/10.1021/acs.est.1c02152
Subramanian G, Parakh P, Prakash H (2013) Photodegradation of methyl orange and photoinactivation of bacteria by visible light activation of persulphate using a tris(2,2′-bipyridyl) ruthenium(II) complex. Photochem and Photobiol Sci 12:456–466. https://doi.org/10.1039/c2pp25316j
Sun Y, Sun S, Wu T et al (2022) Highly effective electrocatalytic reduction of N-nitrosodimethylamine on Ru/CNT catalyst. Chemosphere 305:135414. https://doi.org/10.1016/j.chemosphere.2022.135414
Veerakumar P, Dhenadhayalan N, Lin KC, Liu S, bin, (2015) Highly stable ruthenium nanoparticles on 3D mesoporous carbon: an excellent opportunity for reduction reactions. J Mater Chem A Mater 3:23448–23457. https://doi.org/10.1039/c5ta06875d
von Gunten U (2018) Oxidation processes in water treatment: are we on track? Environ Sci Technol 52:5062–5075. https://doi.org/10.1021/acs.est.8b00586
Xu C, Ming M, Wang Q et al (2018) Facile synthesis of effective Ru nanoparticles on carbon by adsorption-low temperature pyrolysis strategy for hydrogen evolution. J Mater Chem A Mater 6:14380–14386. https://doi.org/10.1039/c8ta03572e
Xu Y, Li C, Lu S et al (2022) Construction of emissive ruthenium(II) metallacycle over 1000 nm wavelength for in vivo biomedical applications. Nat Commun 13:2009. https://doi.org/10.1038/s41467-022-29572-2
Yan Y, Yang Q, Shang Q et al (2022) Ru doped graphitic carbon nitride mediated peroxymonosulfate activation for diclofenac degradation via singlet oxygen. Chem Eng J 430:133174. https://doi.org/10.1016/j.cej.2021.133174
Yang Y, Zhang X, Jiang J et al (2022) Which micropollutants in water environments deserve more attention globally? Environ Sci Technol 56:13–29. https://doi.org/10.1021/acs.est.1c04250
Yin H, Kuwahara Y, Mori K et al (2019a) Plasmonic Ru/hydrogen molybdenum bronzes with tunable oxygen vacancies for light-driven reduction of *p*-nitrophenol. J Mater Chem A Mater 7:3783–3789. https://doi.org/10.1039/c8ta11604k
Yin H, Kuwahara Y, Mori K, Yamashita H (2019b) RuPd alloy nanoparticles supported on plasmonic $HxMoO_3$–y for efficient photocatalytic reduction of *p*-Nitrophenol. Eur J Inorg Chem 2019:3745–3752. https://doi.org/10.1002/ejic.201900801
Yin H, Chen Z, Peng Y et al (2022) Dual active centers bridged by oxygen vacancies of ruthenium single-atom hybrids supported on molybdenum oxide for photocatalytic ammonia synthesis. Angew Chem Int Ed 61:e202114242. https://doi.org/10.1002/anie.202114242
Ying Y, Pumera M (2019) Micro/nanomotors for water purification. Chem Eur J 25:106–121. https://doi.org/10.1002/chem.201804189
Zaoui F, Sebba FZ, Liras M et al (2021) Ultrasonic preparation of a new composite poly(GMA)@Ru/TiO_2@Fe_3O_4: application in the catalytic reduction of organic pollutants. Mater Chem Phys 260:124146. https://doi.org/10.1016/j.matchemphys.2020.124146
Zhang J, Sun B, Guan X et al (2013) Ruthenium nanoparticles supported on CeO_2 for catalytic permanganate oxidation of butylparaben. Environ Sci Technol 47:13011–13019. https://doi.org/10.1021/es402118v
Zhang J, Sun B, Xiong X et al (2014) Removal of emerging pollutants by Ru/TiO_2-catalyzed permanganate oxidation. Water Res 63:262–270. https://doi.org/10.1016/j.watres.2014.06.028
Zhang J, Sun B, Huang Y, Guan X (2015) Catalyzing the oxidation of sulfamethoxazole by permanganate using molecular sieves supported ruthenium nanoparticles. Chemosphere 141:154–161. https://doi.org/10.1016/j.chemosphere.2015.06.088
Zhang G, Huang X, Ma J et al (2021) Ti/RuO_2-IrO_2–SnO_2 anode for electrochemical degradation of pollutants in pharmaceutical wastewater: optimization and degradation performances. Sustainability 13:1–13. https://doi.org/10.3390/su13010126
Zhang B, Xiao X, Chen J et al (2022) Toward fast and durable alkaline hydrogen oxidation reaction on ruthenium. Energy Environ Sci. https://doi.org/10.1039/D2EE02216H
Zhao Y, Luo Y, Yang X et al (2017a) Tunable preparation of ruthenium nanoparticles with superior size-dependent catalytic hydrogenation properties. J Hazard Mater 332:124–131. https://doi.org/10.1016/j.jhazmat.2017.03.004
Zhao Y, Luo Y, Zhu Y et al (2017b) Sensitive colorimetric assay of H_2S depending on the high-efficient inhibition of catalytic performance of Ru nanoparticles. ACS Sustain Chem Eng 5:7912–7919. https://doi.org/10.1021/acssuschemeng.7b01448
Zhao M, Xu L, Vara M et al (2018) Synthesis of Ru icosahedral nanocages with a face-centered-cubic structure and evaluation of their catalytic properties. ACS Catal 8:6948–6960. https://doi.org/10.1021/acscatal.8b00910
Zhou X, Yang Z, Chen Y et al (2022) Single-atom Ru loaded on layered double hydroxide catalyzes peroxymonosulfate for effective E. coli inactivation via a non-radical pathway: efficiency and mechanism. J Hazard Mater 440:129720. https://doi.org/10.1016/j.jhazmat.2022.129720
Zhu K, Xu X, Xu M et al (2021a) One-pot synthesis of tensile-strained PdRuCu icosahedra toward electrochemical hydrogenation of alkene. ChemElectroChem 8:3855–3862. https://doi.org/10.1002/celc.202100827
Zong Y, Zhang H, Zhang X et al (2021) Highly selective oxidation of organic contaminants in the Ru^{III}-activated peroxymonosulfate process: the dominance of Ru^{V}=O species. Chemosphere 285:131544. https://doi.org/10.1016/j.chemosphere.2021.131544